J Mar Sci Technol (2002) 6:193–204

Journal of
Marine Science
and Technology


# Comparison of numerical and experimental results of nonlinear wave-induced vertical ship motions and loads

Nuno Fonseca and Carlos Guedes Soares

Unit of Marine Technology and Engineering, Technical University of Lisbon, Instituto Superior Técnico, Av. Rovisco Pais, 1049-001 Lisbon, Portugal

**Abstract** A nonlinear time-domain procedure is presented which is used to calculate the vertical responses of a container ship advancing in head waves. The method assumes linear radiation forces represented by time convolution of memory functions, infinite frequency added masses, and radiation restoring coefficients. The nonlinear hydrostatic restoring and Froude–Krilov forces are computed exactly over the instantaneous wetted surface of the ship's hull. Forces due to green water on deck are calculated using the momentum method. Nonlinear effects are identified on different vertical ship responses, namely on the heave and pitch motions, the vertical accelerations, and the vertical bending moment. These nonlinear effects are expressed by the variation of the transfer function with the wave amplitude, the higher-order harmonics of the time signals, the offset of the time series, and the asymmetry of the peaks. The numerical results and the quantified nonlinear effects are compared with experimental results showing an ability to reproduce the main nonlinear effects.

**Key words** Vertical motions and loads · Nonlinear · Experimental data · Time simulation

## 1 Introduction

It is known that ships with fine forms, or small block coefficients, may experience wave-induced vertical loads that are highly asymmetric. This means, for example, that the sagging moment peaks may be much larger than the hogging ones. The importance of these nonlinear effects is reflected by the Classification Society rules, which suggest empirical formulae for determining the wave-induced design bending moment differently for sagging and hogging conditions.

The nonlinearities mentioned above are mostly associated with the "nonlinear geometry" of the hull, where the ship's sides have considerable flare on both the bow and the stern areas. Ships of this type are container ships, frigates, some passenger ships, etc., which combine the requirements of relatively fast speeds with large cargo and internal volumes and also a large deck area. For these reasons, the underwater hull is fine and the volume and the deck area are obtained with a large flare up to deck level. Furthermore, the flare on the bow helps fast ships to keep their decks drier.

There is experimental evidence, mainly from model tests but also from full-scale measurements, that nonlinear effects are important for the vertical ship responses, and particularly for the vertical bending moment of small block coefficient ships. Results from model tests[1,2] show that the sagging peaks of the vertical bending moment may be twice as large or more than the hogging peaks, and the differences increase for models with smaller block coefficients. Murdey[3] and Nethercote[4] obtained similar results for models of series 60 ships and a frigate.

Watanabe et al.[5] presented a more systematic study of the nonlinear effects on the vertical bending moment on a container ship advancing in head regular and irregular waves. As well as the asymmetry of the bending moment, the harmonic content of the signals measured and the mean values were determined. It was concluded that all these nonlinear characteristics are present in the measured vertical bending moment.

O'Dea et al.[6] conducted experimental tests with a model of the same containership with the objective of determining the influence of the wave steepness on the vertical motions and accelerations. In regular waves, it was observed that the higher harmonic content of the responses is small, but around the resonance frequency, the first harmonics normalized by the wave amplitude tend to decrease with greater wave steepness.

Few full-scale measurements have been published, but Smith[7] and Hay et al.,[8] for example, presented the results of stresses measured on board a frigate sailing in moderate to severe sea states. The results clearly show

*Address correspondence to:* C. Guedes Soares
(e-mail: guedess@alfa.ist.utl.pt)
Received: December 17, 2001 / Accepted: January 31, 2002

that the sagging stresses are much higher than the hogging ones for low probability levels.

Since it is recognized that nonlinear effects are important for certain types of ship and cannot be neglected in hydrodynamic-based calculations of design wave loads, there have been efforts to develop methods to calculate the nonlinear seakeeping of ships in waves. Some methods have been proposed which are based on partially nonlinear formulations, with the objective of giving practical solutions, but there have also been attempts to solve the fully nonlinear problem.

A fully nonlinear solution has been attempted by assuming both viscous and inviscid flow. Assuming a viscous fluid, Wilson et al.[9] applied a Reynolds averaged Navier–Stokes (RANS) code to compute the viscous flow around two ships subjected to regular incident waves. Although some results of the wave elevation around the ships were presented, numerical problems still exist and the computational effort is huge.

Beck et al.,[10] Scorpio et al.,[11] and Subramani et al.[12] followed a different approach, assuming an ideal fluid and based on the Euler–Lagrange method together with a representation of the hull and a free surface boundary by desingularized Rankine sources. Some partial results have been presented, but numerical problems still exist and the computational effort is also huge. One can say that fully nonlinear solutions are still under development, and will not be available for practical applications in the near future.

Partial nonlinear methods are based on potential flow, and some degree of linearization is assumed in the solution of the hydrodynamic problem, but the equations of motion and loads include nonlinear terms. More complete methods do exist, but they are less practical for use in routine applications. These are based on time domain panel methods, using Green functions and discretizing only the hull surface,[13,14] or Rankine sources distributed over the hull and free surface.[15,16] In these methods, the body boundary condition may be nonlinear by being satisfied at the exact position at each time instant, but the free surface is linearized.

More practical methods have been proposed by Xia and Wang[17] and Fonseca and Guedes Soares,[18,19] which are based on time domain strip theories where the linear radiation forces are represented by the convolution of memory functions. Froude–Krilov and hydrostatic forces are computed instantaneously over the wetted hull surface. Additional nonlinear terms may be introduced in the equations of motions, such as slamming forces and water-on-deck forces.

Watanabe and Guedes Soares[20] presented comparative calculations for an S175 container ship using six different simplified, partially nonlinear codes. Head regular waves, three wavelengths, and two wave heights were considered. The results presented included vertical motions, accelerations, and vertical bending moments. Details of the approximations used by each of the codes were presented in tabular form to make it easy to compare the code assumptions. For low wave heights, most of the results agree with each other and with linear strip theory to within approximately 10%. For larger wave heights, substantial differences were observed between the predictions from the different codes, but the origin of these differences is not clear.

The ISSC 1997 Committee on Loads[21] and the ISSC 2000 Committee VI.1 on Extreme Loads[22] concluded that these type of methods may be appropriate to predict nonlinear loads on ships, but validation is necessary, which includes comparisons with nonlinear experimental data.

In this paper, the method developed by Fonseca and Guedes Soares[18,19] is used to make systematic computations of the nonlinear vertical motions and loads on a container ship. The nonlinear characteristics of the responses are identified and compared with published experimental data.

## 2 Numerical model

The formulation on which the numerical model is based was developed by Fonseca and Guedes Soares.[18] That publication presents some calculated results for a ship advancing in regular waves. The method was also generalized for irregular seas.[19] Here, the formulation will be described briefly to provide the background of the method, which will be required for the discussion of the results.

A coordinate system fixed with respect to the mean position of the ship is defined, $X = (x,y,z)$, with $z$ in the vertical upward direction and passing through the center of gravity of the ship, $x$ in the longitudinal direction of the ship and pointing to the bow, and $y$ perpendicular to the latter and in the port direction. The origin is in the plane of the undisturbed free surface.

The solution of the hydrodynamic problem assumes that the flow is inviscid, the hull is slender, the forward speed is small, and the amplitudes of the incident waves and unsteady motions are small enough. Considering a ship advancing in waves and oscillating as an unrestrained rigid body: the oscillatory motions will consist of three translations and three rotations. Here, only head waves will be considered, and it is assumed that the longitudinal (fore–aft) hydrodynamic unsteady forces are negligible, which is the basis of the strip-theory assumptions. Therefore, the ship will only heave and pitch.

Equating the hydrodynamic external forces to the mass and gravity forces, one obtains the equations of motion. These equations, which combine linear and

nonlinear terms, are solved in the time domain by a numerical procedure. For heave and pitch the equations are

$$\left(M+A_{33}^{\infty}\right)\ddot{\xi}_3(t)+\int_{-\infty}^{t}\left[K_{33}^{m}(t-\tau)\dot{\xi}_3(\tau)\right]\mathrm{d}\tau+C_{33}^{m}\xi_3(t)+A_{35}^{\infty}\ddot{\xi}_5(t)+\int_{-\infty}^{t}\left[K_{35}^{m}(t-\tau)\dot{\xi}_5(\tau)\right]\mathrm{d}\tau+C_{35}^{m}\xi_5(t)+F_3^{\mathrm{H}}(t)-Mg+F_3^{gw}(t)=F_3^{\mathrm{D}}(t)+F_3^{\mathrm{K}}(t) \quad (1)$$

$$\left(I_{55}+A_{55}^{\infty}\right)\ddot{\xi}_5(t)+\int_{-\infty}^{t}\left[K_{55}^{m}(t-\tau)\dot{\xi}_5(\tau)\right]\mathrm{d}\tau+C_{55}^{m}\xi_5(t)+A_{53}^{\infty}\ddot{\xi}_3(t)+\int_{-\infty}^{t}\left[K_{53}^{m}(t-\tau)\dot{\xi}_3(\tau)\right]\mathrm{d}\tau+C_{53}^{m}\xi_3(t)+F_5^{\mathrm{H}}(t)+F_5^{gw}(t)=F_5^{\mathrm{D}}(t)+F_5^{\mathrm{K}}(t) \quad (2)$$

where $\xi_3$ and $\xi_5$ represent the heave and pitch motions, respectively, and the dots over the symbols represent differentiation with respect to time. $M$ is the ship's mass, $g$ is the acceleration due to gravity, and $I_{55}$ represents the ship's inertia about the $y$-axis. The hydrostatic force and moment, $F_3^{\mathrm{H}}$ and $F_5^{\mathrm{H}}$, respectively, are calculated at each time step by integration of the hydrostatic pressure over the wetted hull under the undisturbed wave profile. The exciting forces due to the incident waves are decomposed into a diffraction part, $F_k^{\mathrm{D}}$, and the Froude–Krilov part $F_k^{\mathrm{K}}$. The diffraction part, which is related to the scattering of the incident wave field due to the presence of the moving ship, is kept linear. It results from the solution of the hydrodynamic problem of the ship advancing with constant speed through the incident waves and being restrained at her mean position. Since this is a linear problem and the exciting waves are known a priori, it can be solved in the frequency domain and the resulting transfer functions can be used to generate a time history of the diffraction heave force and pitch moment. The transfer functions are calculated by a strip method.

The Froude–Krilov part is related to the incident wave potential, and results from the integration at each time-step of the associated pressure over the wetted surface of the hull under the undisturbed wave profile.

The radiation forces, which are calculated using a strip method, are represented in the time domain by infinite frequency added masses $A_{kj}^{\infty}$, radiation restoring coefficients $C_{kj}^{m}$, and convolution integrals of memory functions $K_{kj}^{m}$(t). The radiation restoring forces, associated with the restoring coefficients, represent a correction to the hydrodynamic steady forces acting on the ship due to the steady flow. The convolution integrals represent the effects of the whole past history of the motion, accounting for the memory effects due to the radiated waves. The memory functions and the radiation restoring coefficients are obtained by relating the radiation forces in the time domain and in the frequency domain by means of Fourier analysis.

Finally, the vertical forces associated with the green water on deck $F_k^{gw}$(t), which occurs when the relative motion is larger than the free board, are calculated using the momentum method. This way the hydrodynamic pressure on the deck includes three terms: the hydrostatic pressure, one term that accounts for the variation of the mass of water on the deck, and one term associated with the acceleration of the deck.

The wave-induced structural dynamic loads at a cross section are given by the difference between the inertia forces and the sum of the hydrodynamic forces acting on the part of the hull forward of that section. The vertical shear force and vertical bending moment, respectively, are given by

$$V_3(t)=I_3(t)-R_3(t)-D_3(t)-K_3(t)-H_3(t)-G_3(t) \quad (3)$$

$$M_5(t)=I_5(t)-R_5(t)-D_5(t)-K_5(t)-H_5(t)-G_5(t) \quad (4)$$

where $I_k$ represents the vertical inertia force (or moment) associated with the ship's mass forward of the cross section under study. As assumed for the calculation of the ship's motions, the radiation ($R_k$) and diffraction ($D_k$) hydrodynamic contributions for the loads are linear, and the Froude–Krylov ($K_k$) and hydrostatic ($H_k$) contributions are nonlinear since they are calculated over the "exact" wetted hull surface at each time step. $G_k$ represents the contribution to the structural loads of the forces of the green water on deck.

The formulation to calculate all contributions to the loads is consistent with the formulation applied to solve the unsteady motion problem. The convention for the loads is such that the sagging shear force and hogging bending moment are positive.

## 3 Comparison between numerical and experimental results

Experimental sea-keeping tests with scaled ship models have been carried out during the last four decades in order to obtain data to validate theoretical and numerical sea keeping methods. Some of these experimental data have been published, but most of these results are not adequate when the object is to investigate the nonlinear responses of ships subjected to large-amplitude waves. This is because the results are usually presented in the form of transfer functions, defined by the amplitude of the first harmonic of the response divided by the

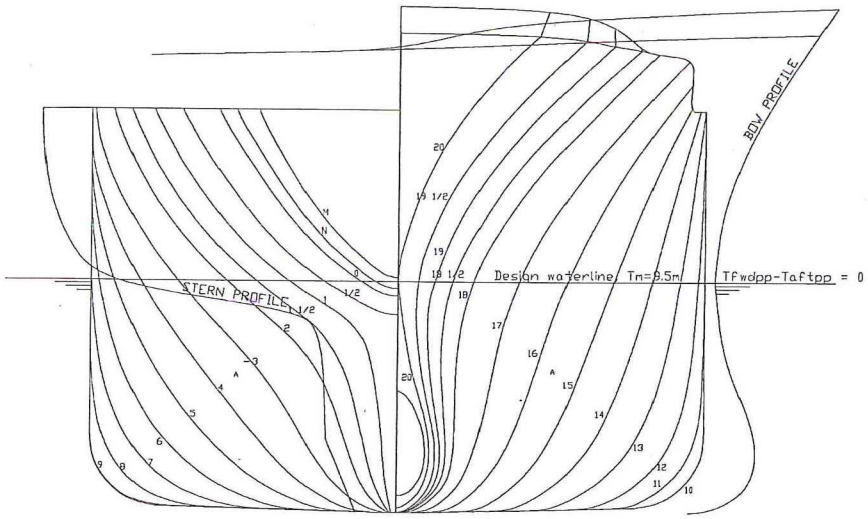


**Fig. 1.** Bodylines of the S-175 container ship

first harmonic of the incoming wave, together with the phase angle of the first harmonic. Usually, all nonlinear effects are lost, and the results are suitable to validate linear methods.

O'Dea et al.[6] and Watanabe et al.[5] are among the few authors who have published experimental data on the vertical responses of ship models to regular and irregular waves, with an emphasis on the nonlinear effects. Both authors tested models of the S-175 container ship. These experimental results will serve has a benchmark to evaluate the quality of the predictions of the numerical model.

### *3.1 Characteristics of the ship*

The S-175 container ship is well known because it was used by the 15th ITTC[23] and the 16th ITTC[24] to carry out a comparative numerical study of linear wave-induced motions and structural loads. The database that resulted from that study includes numerical results from many institutions, and also some experimental data. The ship's hull has a pronounced flare on the bow and the stern, and therefore it is expected that large nonlinear effects are associated with the vertical motions. Figure 1 shows the ship's bodylines, Table 1 lists the main particulars, and Fig. 2 shows the weight distribution used by Watanabe et al.[5]

### *3.2 Vertical motions and accelerations*

O'Dea et al.[6] conducted an experimental program with a model of the S-175 with the objective of identifying nonlinear effects on the vertical motions. Some of the tests were carried out in head regular waves, for two speeds of advance ($F_n$ = 0.20 and $F_n$ = 0.275), three wavelengths ($\lambda/L_{pp}$ = 1.0, 1.2, and 1.4), and several wave

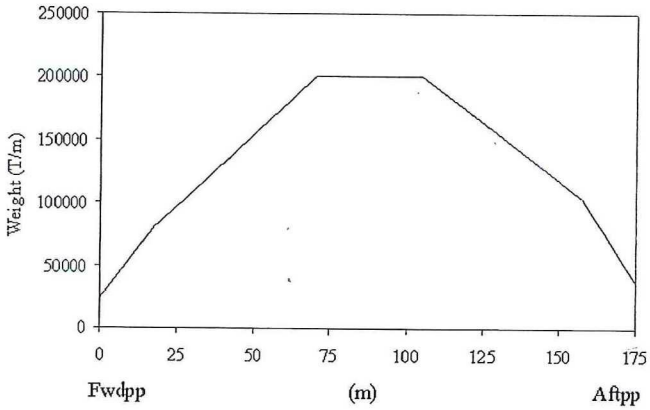


**Fig. 2.** Longitudinal weight distribution of the model

**Table 1.** Main particulars of the S-175 container ship

| | | |
|---|---|---|
| Length between perpendiculars | $L_{pp}$ (m) | 175.0 |
| Beam | $B$ (m) | 25.40 |
| Depth | $D$ (m) | 15.40 |
| Draft | $T$ (m) | 9.50 |
| Displacement | $\Delta$ (ton) | 24742 |
| Long position of CG | $LCG$ (m) | –2.43 |
| Block coefficient | $C$b | 0.5716 |
| Pitch radius of gyration | $K_{yy}/L_{pp}$ | 0.24 |

amplitudes between $L_{pp}/240$ and $L_{pp}/40$. The resonance of the vertical motions occurs at approximately $\lambda/L_{pp}$ = 1.2, $F_n$ represents the Froude number, $\lambda$ the wavelength, and $L_{pp}$ the length between perpendiculars.

Measurements were taken of the heave and pitch motions, and of the vertical acceleration on the bow at a point located at 0.15 $L_{pp}$ aft of the forward perpendicular. To identify the nonlinear effects, the authors applied Fourier analysis to the signals measured in order

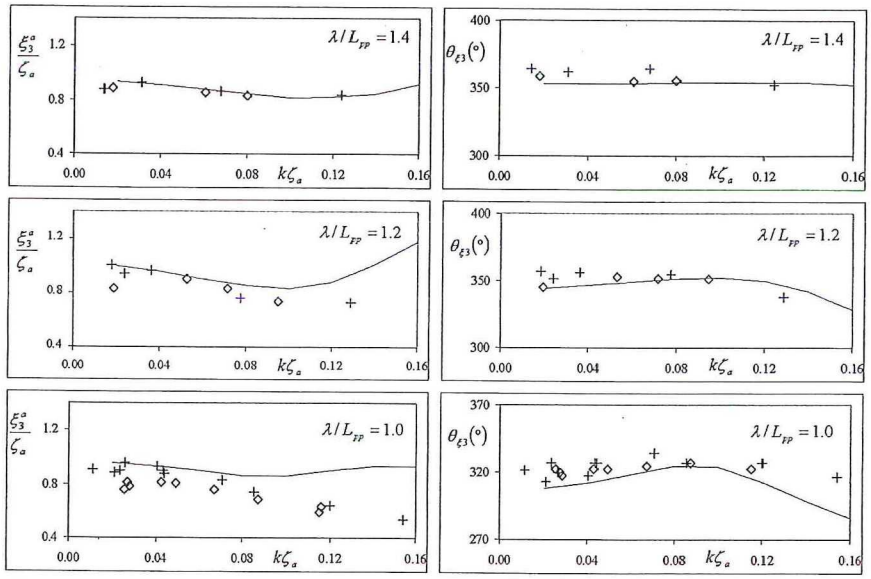


**Fig. 3.** Heave motion. Amplitudes and phase angles of the first harmonic. Comparison between experimental and numerical results ($F_n = 0.20$, $\beta = 180°$)

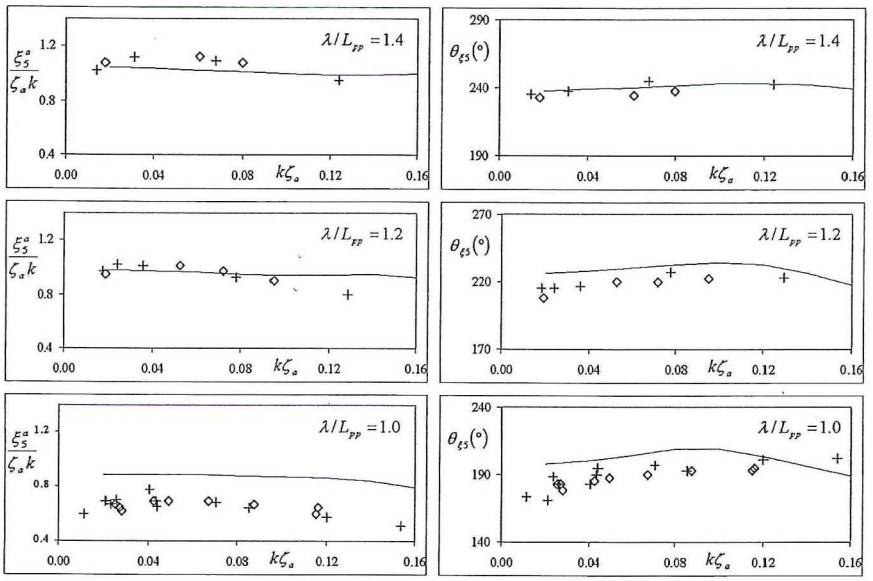


**Fig. 4.** Pitch motion. Amplitudes and phase angles of the first harmonic. Comparison between experimental and numerical results ($F_n = 0.20$, $\beta = 180°$)

to obtain the amplitudes and phase angles of the harmonic components.

The next figures present the comparisons between experimental results (symbols) and the numerical results (lines). Different symbols are used to identify two groups of tests conducted at periods separated by 1 year. Each graph presents results corresponding to one wavelength as function of the wave slope.

Figures 3–5 show the amplitudes and phase angles of the first harmonics of heave, pitch, and vertical acceleration, respectively. The results are for $F_n = 0.20$, and are presented as function of the wave slope, $k\zeta_a$, where $k$ is the wave number and $\zeta_a$ is the wave amplitude. Heave amplitudes are nondimensionalized by the wave amplitude, pitch amplitudes by the wave slope, and the vertical acceleration at the bow amplitudes by $g\zeta_a/L_{pp}$. The phase angles are in degrees, and represent the delay of the first harmonic with respect to the maximum wave elevation at the origin of the coordinate system.

Heave experimental nondimensional amplitudes show a significant decrease with an increase of the wave slope, especially for the two shorter wavelengths. The reduction is up to around 40% for $\lambda/L_{pp} = 1.0$. This nonlinear effect is very well captured by the numerical model for wave slopes up to approximately 0.10. There are discrepancies for higher wave amplitudes, since the tendency of the numerical results seems to be contrary to the experiments. For the two shorter wavelengths,

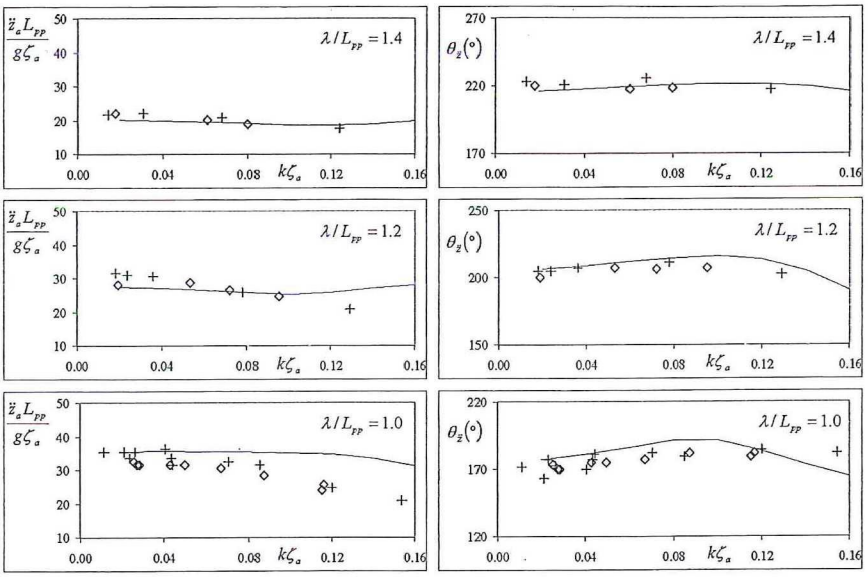


**Fig. 5.** Vertical acceleration at the bow. Amplitudes and phase angles of the first harmonic. Comparison between experimental and numerical results ($F_n = 0.20$, $\beta = 180°$)

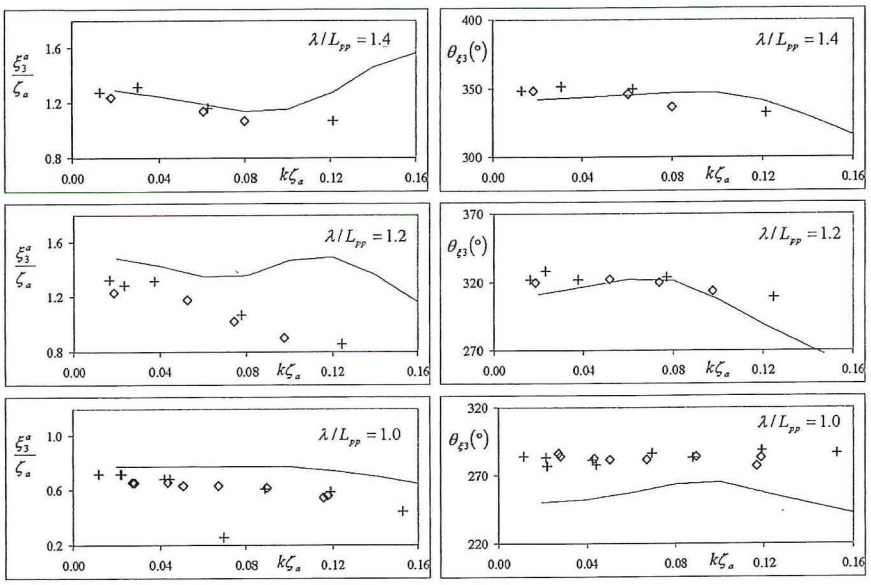


**Fig. 6.** Heave motion. Amplitudes and phase angles of the first harmonic. Comparison between experimental and numerical results ($F_n = 0.275$, $\beta = 180°$)

the numerical results slightly overestimate the experiments. With respect to the phase angles, the experimental data seem to be independent of the wave slope. The calculated results compare well with the experiments.

The pitch nondimensional amplitudes are less sensitive to the wave slope, although there is a small reduction with the wave slope. The numerical results compare well with the experiments, except for the shorter wavelength where they overestimate the measured results. Unlike heave, the experimental pitch phase angles tend to increase with the wave amplitude, with variations up to 30°. In general, this tendency is well represented by the numerical results. The nondimensional amplitudes of the vertical accelerations at the bow reduce with the wave slope, a characteristic that is captured by the numerical model.

Figures 6–8 represent ship's responses which are similar to those described in the previous paragraphs, but for a higher Froude number ($F_n = 0.275$). The observations for $F_n = 0.20$ concerning the experimental data can be used to describe Figs. 6–8, since the conclusions are similar. However, with respect to the numerical results, the comparisons are, in general, worse. One can say that the problems identified previously for the lower Froude number are now amplified. In particular, the heave amplitudes in the higher wave steepness range largely exceed those found in the experiments, and in general

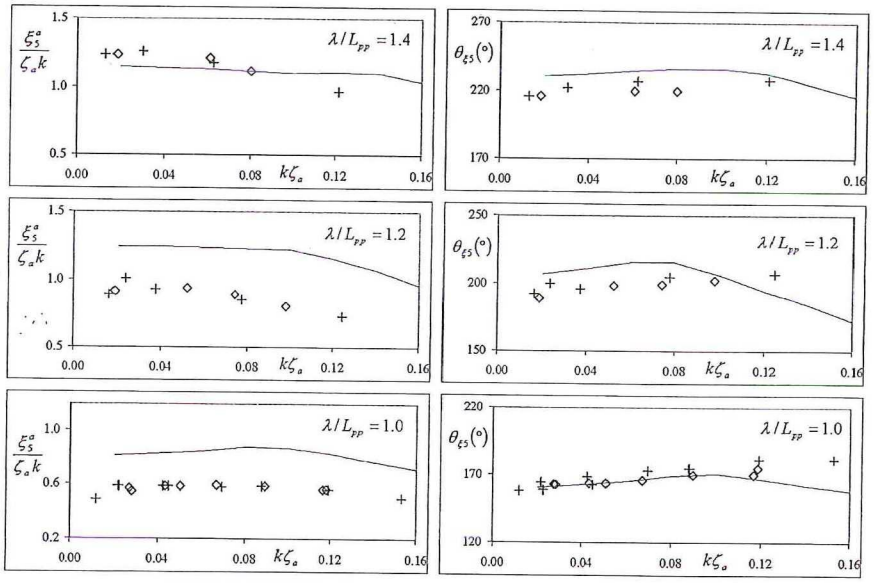


**Fig. 7.** Pitch motion. Amplitudes and phase angles of the first harmonic. Comparison between experimental and numerical results ($F_n = 0.275$, $\beta = 180°$)

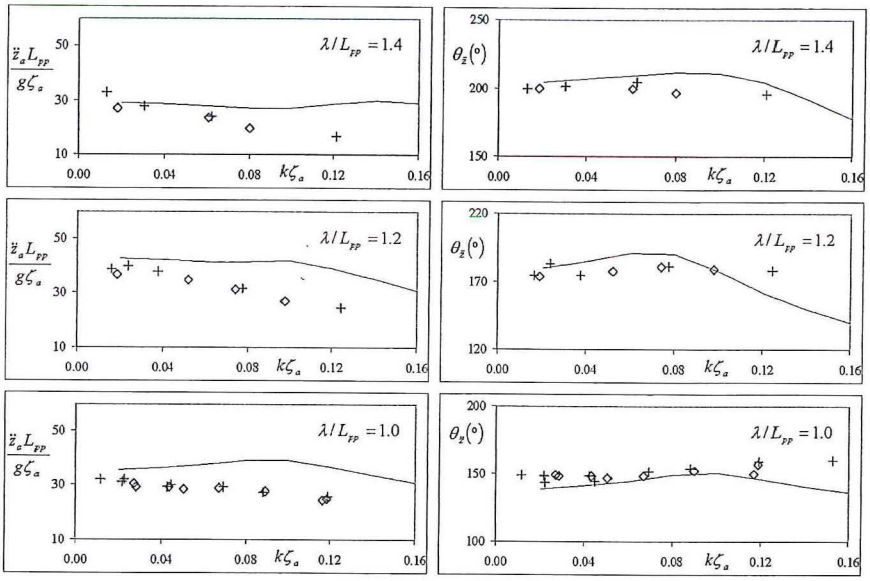


**Fig. 8.** Vertical acceleration at the bow. Amplitudes and phase angles of the first harmonic. Comparison between experimental and numerical results ($F_n = 0.275$, $\beta = 180°$)

all vertical response amplitudes are above the experimental points for the two shorter wavelengths.

The worsening of the numerical predictions for the higher Froude number reveals the limitations of the strip theory to represent the forward speed effects correctly. In fact, the forward speed effects on the radiation and diffraction forces only account for the steady flow at infinity, together with the angle between this flow and the hull. All perturbations due to the hull, and interactions between these perturbations and the oscillatory flow are neglected. Theoretically, this assumption is valid for slender ships advancing at low speed.

Another aspect is the deviation of the numerical amplitudes of heave from the experimental data for the higher-amplitude waves. It is believed that the limitation here is not simply the strip method itself, but also the theoretical model that represents the nonlinear effects associated with the vertical motions. The assumption of this model is that the dominant nonlinear contributions arise from the hydrostatic and Froude–Krilov components, and therefore these components are calculated at each time instant and account for the "exact" hull wetted surface. The assumption seems to be adequate for medium to large amplitude waves, but not for very large waves.

In fact the conditions where the numerical model fails are extremely severe and unrealistic. For example, in the graphs in Fig. 6, the ship advances with a relatively

high speed ($F_n$ = 0.275), in regular waves with double amplitudes almost equal to the ship's draft, and the waves induce resonant heave motion. It is possible that for these conditions, the nonlinear effects on the radiation and diffraction forces have some influence on the calculation of the resonance heave amplitude.

In addition, the viscous effects due to the separation of flow during the upward vertical motion of the hull may have some influence. Preliminary simulations of the ship's motions accounting for viscous effects associated with the relative motions seem to indicate that the vertical viscous forces reduce the resonance heave amplitude, thus shortening the gap between calculations and experimental results. The calculation of viscous forces is based on an empirical model.

Another characteristic of the nonlinear responses is the presence of higher harmonics on the time signals. In the case of heave and pitch motions, the magnitude of the higher harmonics is small. According to O'Dea et al.,[6] the magnitudes of the second and third harmonics of the measured vertical motions are around 1% to 2% of the first harmonics. On the other hand, the vertical accelerations are more sensitive to the existence of higher harmonics. In fact, the second derivative of the first three harmonics of the accelerations with respect to time in effect multiplies the displacements by $\omega^2$, $4\omega^2$, and $9\omega^2$, respectively. This means that, compared with the motions, the importance of the second and third harmonics is 4 and 9 times larger, respectively, for the accelerations. Experimental results show that for the largest wave amplitude, the second and third harmonics of the vertical accelerations account for 20% and 8%, respectively, of the first harmonic.

The numerical model is able to capture these nonlinear effects, but there are some discrepancies. Figure 9 shows the second and third harmonics of the vertical acceleration at the bow as a function of the wave slope for $F_n$ = 0.20 and head regular waves with $\lambda/L_{pp}$ = 1.0. The results are normalized by the acceleration due to gravity, $g$, the symbols represent experimental results, and the lines represent numerical results. Regarding the second harmonics, the tendency of the calculated results is correct up to the range of large wave slopes, but the experimental data is overestimated.

Above $ka$ = 0.10–0.12, the tendency of the curve changes and the magnitude of the second-order effects reduces, which is contrary to the experiments. The reason may be related to the effects on the bow of the green water on deck. In fact the change in the tendency of the calculated curve occurs for wave slopes where the relative motion at the bow is larger than the free board, and thus green water on the deck starts. According to the numerical model, from the instant that the free surface of the wave crosses the line of the deck, not only does the vertical upward impulsion force cease to increase, but the downward force of green water on the deck begins. This affects the characteristics of the vertical acceleration. Certainly these effects also occur in the experiments, and one does not see a drop in the second harmonics of the experimental data for large wave slopes, which may mean that the mathematical model does not correctly represent reality.

In general, the numerical line of the third harmonic components compares better with the experimental data.

### 3.3 *Vertical bending moment*

Watanabe et al.[5] tested the S-175 to investigate the influence of the bow flare on the shipping of water on the bow deck, and on the asymmetry and higher-order effects of the wave-induced vertical bending moment. Two models, 4.5 m long, and with different bows, were tested. One had the standard S-175 original bow shape (O-model), while the other had a modified bow with more flare and a greater volume above the waterline (M-model). Figure 10 shows the cross-section lines and bow profile of both models.

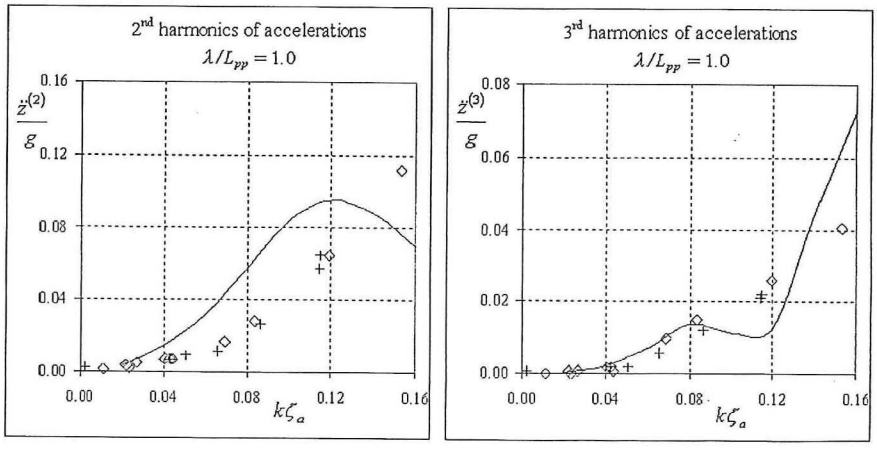


**Fig. 9.** Second and third harmonics of the vertical acceleration at the bow as a function of the wave slope ($F_n$ = 0.20, $\beta$ = 180°, $\lambda/L_{pp}$ = 1.0)

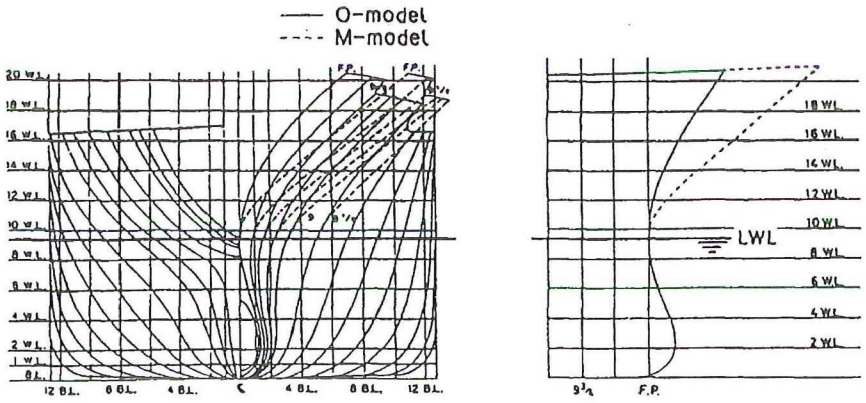


**Fig. 10.** Bodylines of the original S-175 (O-model) and the modified S-175 (M-model)[5]

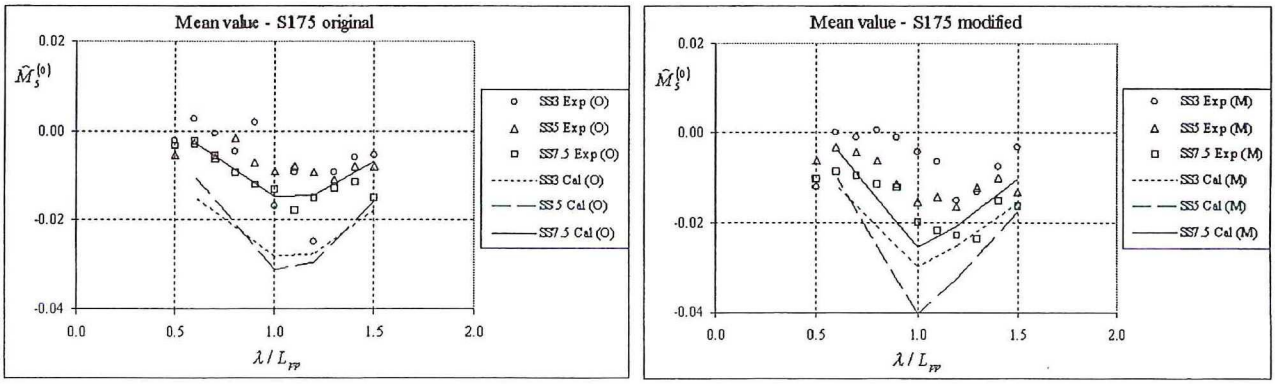


**Fig. 11.** Comparison of experimental and calculated mean offset of the vertical bending moment at three cross sections. Results for original and modified S-175. $F_n = 0.25$, $\beta = 180°$, $\zeta_a = 0.31T$

Watanabe et al.[5] present the results of tests conducted in head regular waves for the whole wavelength range of interest, and a Froude number of 0.25. The wave amplitude was kept constant and equal to $0.31T$, where $T$ is the mean draft. The results include measured data of the pitch motion, relative motion and vertical acceleration at the bow, impact pressures at several points, and vertical bending moment at six positions along the ship's length. The signals of the vertical bending moment were analyzed to extract the mean offset and the magnitudes of the first and second harmonics. In addition, tests were carried out for one irregular long-crested sea-state.

Figures 11–13 show the results of the mean offset, and of the first and second harmonics, respectively, of the vertical bending moment at three cross sections (SS3, SS5, SS7.5) of the original and modified S-175. The sections are numbered on a reference system from 0 (aft perpendicular) to 10 (forward perpendicular). The results are presented as a function of the nondimensional wavelength ($\lambda/L_{pp}$). The symbols stand for experimental data, and the lines for the calculated results.

Starting with the mean values of the vertical bending moment in Fig. 11, these magnitudes are nondimensionalised by $\rho g B L_{pp}^2 \zeta_a^2/T$. The experimental results are larger around the wave frequencies that induce the vertical motion resonance. In terms of magnitude, the mean offset at section 7.5 (on the bow) comes to around 50% of the first harmonic, revealing the strong nonlinear behavior of this response. The numerical results compare very well with the experimental ones for section 7.5, but largely exceed the experimental ones for the other two sections. The measured mean offset is larger for the modified model than for the original, behavior that is well predicted by the numerical model.

The amplitudes of the first harmonics of the bending moment are shown in Fig. 12, where the nondimensional values are $\widehat{M}_5^a = M_5^a/(\rho g B L_{pp}^2 \zeta_a^2)$. In this case, one can observe that the influence of the bow shape on the experimental data is small. The calculated results exceed those of the experiments and are larger for the modified model.

With respect to the second harmonics (Fig. 13), their magnitudes are non-dimensionalized by the mean values. The experimental results show that their magnitudes reach large values for the wave frequency range around the resonance of the vertical motions. The mag-

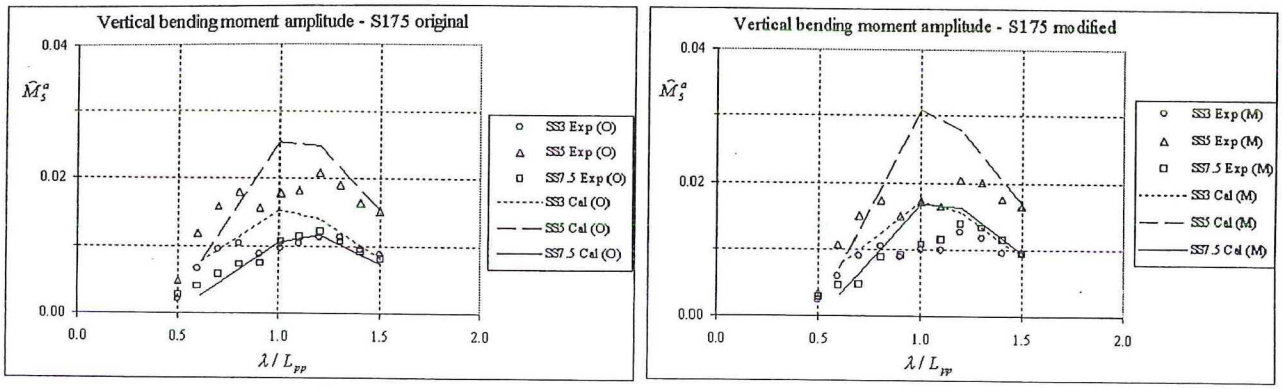


**Fig. 12.** Comparison of experimental and calculated first harmonics of the vertical bending moment at three cross sections. Results for original and modified S-175. $F_n = 0.25$, $\beta = 180°$, $\zeta_a = 0.31T$

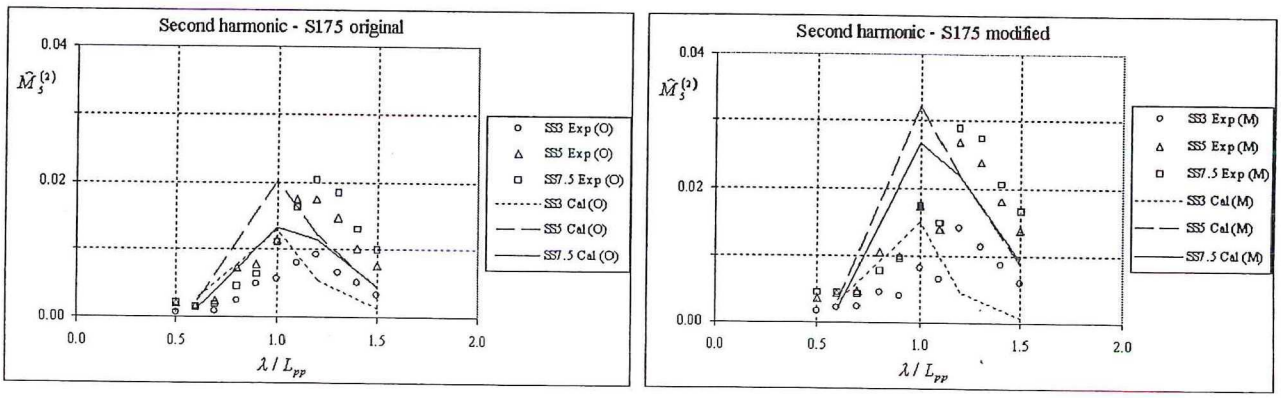


**Fig. 13.** Comparison of experimental and calculated second harmonics of the vertical bending moment at three cross sections. Results for original and modified S-175. $F_n = 0.25$, $\beta = 180°$, $\zeta_a = 0.31T$

nitude of the second harmonic comes to 60% of that of the first harmonic in the case of the modified model. These nonlinear effects are larger for the modified model. In general, the numerical results compare reasonably well with the experiments, although the predicted peak occurs for a smaller wavelength.

Figure 14 shows the distribution along the ship's length of the sagging (negative) and hogging (positive) peaks of the vertical bending moment. The model advances with $F_n = 0.25$ in head regular waves with $\lambda/L_{pp} = 1.2$ and $\zeta_a = 0.31T$. The open and closed symbols stand for the experimental results of the original and modified S-175, respectively. The broken and continuous lines represent the numerical results for the original and modified hull, respectively. Moments are nondimensionalised as $\hat{M}_5 = M_5/(\rho g B L_{pp}^2 \zeta_a)$.

The experimental results clearly show the influence of the bow shape on the sagging peaks, which are larger for the modified S-175, especially between the bow and midship. On the other hand, the bow shape has a small influence on the hogging peaks. In this case, the calculated results compared very well with the experiments, and the method is able to represent correctly the influence of the bow shape on the peaks of the bending moment.

Finally, Fig. 15 presents the distribution along the ship's length of the vertical bending moment peaks induced by an irregular sea state. The model advances with $F_n = 0.25$ in head irregular waves with a mean wave period of $T_z = 11.1$ s and significant wave height of $H_S = 8.33$ m. The representation of the results is similar to that in Fig. 14, but the moments now represent significant values $(\hat{M}_5)_{1/3}$, defined by the average of the third largest peaks. The moments are nondimensionalised by $\rho g B L_{pp}^2 H_S/2$. An analysis of the experimental results and a comparison with the predictions leads to the same conclusions as presented for Fig. 14, although now the predicted sagging peaks are slightly lower than the experimental results from the midship to the bow region.

The asymmetry of the bending moment peaks, which was obtained experimentally in both regular and irregu-

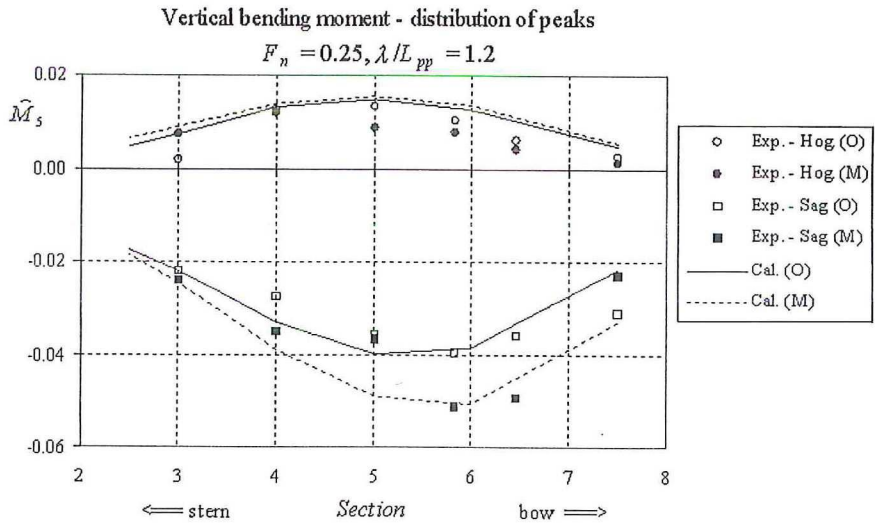


**Fig. 14.** Distribution of the hogging (positive) and sagging (negative) peaks along the ship's length. Experimental and calculated results for the original and modified S-175. $F_n = 0.25$, $\beta = 180°$. Regular waves with $\lambda/L_{pp} = 1.2$, $\zeta_a = 0.31T$

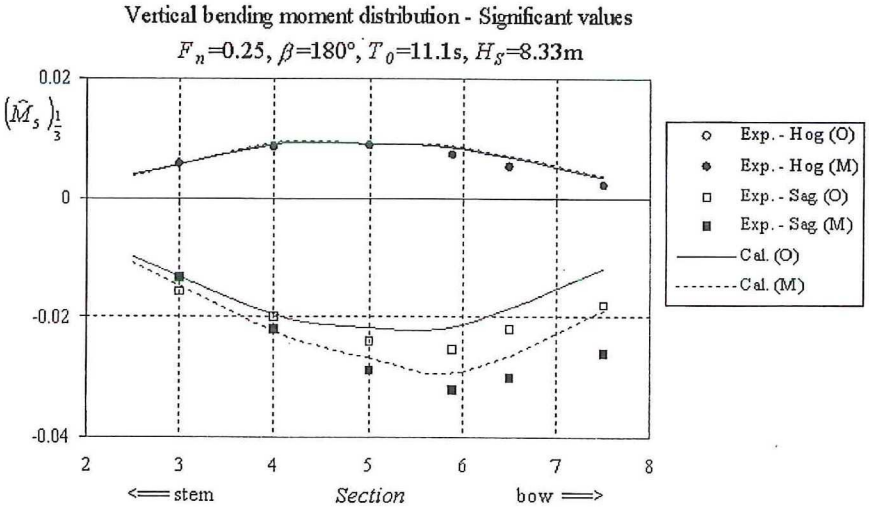


**Fig. 15.** Distribution of significant hogging (positive) and sagging (negative) peaks along the ship's length. Experimental and calculated results for the original and modified S-175. $F_n = 0.25$, $\beta = 180°$. Irregular waves with $T_0 = 11.1$s and $H_S = 8.33$m

lar waves and can be well predicted by the numerical model, is associated with the hull shape, which has significant flare on the bow and the stern. In fact, because of the large flare above the still waterline, the variation of the impulsion forces, which is given by the contribution of the hydrostatics and Froude–Krilov pressures, is larger when the ship's bow submerges than when the bow emerges. This results in a greater sagging moment than hogging moment.

As a final observation, one can say that, in the test conditions, the numerical method is able to predict the peaks of the vertical bending moment with a good level of accuracy. The higher-order effects, such as the mean offset of the signals and second-order harmonics, can be identified by the method, but there are some discrepancies. These discrepancies may indicate that the theoretical model does not correctly, or completely, represent the physics of the phenomena involved.

## 4 Concluding remarks

A partially nonlinear time-domain procedure is presented, and is used to calculate the vertical responses of a container ship advancing in head waves. Nonlinear effects are identified on different vertical ship responses, and are systematically compared with experimental data published previously.

Comparisons of the transfer functions of the heave, pitch, and vertical acceleration at the bow show that the numerical method is able to capture the reduction in the nondimensional amplitudes with the increase in the wave amplitude, except in the higher wave amplitude range, where the calculated results exceed those of the experiments. The phase angles are also well predicted, including the nonlinear variation of the pitch phases with the wave amplitude. The worst results are for the higher Froude number, reflecting the limitations

of strip theory to represent the forward speed effects. Higher-order effects on the vertical accelerations are reasonably well represented by the calculation method, but there are discrepancies for the higher wave amplitudes.

With respect to the vertical bending moment, the numerical method is able to capture all nonlinear effects observed in the experimental data. However, there are some discrepancies on the mean offset and first harmonics where the calculations exceed the experimental results. Second harmonics are reasonably well predicted, although the numerical peaks occur for frequencies a little higher than those of the experimental curves. The distribution of peaks along the ship's length is very well predicted, in both regular and irregular waves.

*Acknowledgments.* The first author is grateful to the Fundação para a Ciência e a Tecnologia for having provided a scholarship, which has supported him during the development of the theoretical work. This work was partially developed within the research project WAVELOADS (Advanced Methods to Predict Wave Induced Loads for High Speed Ships), which was partially financed by the European Commission through the contract BRPR-CT-97-0580.

## References

1. Dalzell JF (1962) Cross-spectral analysis of ship model motions: a destroyer model in irregular long-crested head seas. Rep 810, Davidson Laboratory, Stevens Institute of Technology
2. Dalzell JF (1962) Some further experiments on the application of linear superposition techniques to the responses of a destroyer model in extreme long-crested head seas. Rep 819, Davidson Laboratory, Stevens Institute of Technology
3. Murday DC (1972) An analysis of longitudinal bending moments measured on models in head waves. Trans R Inst Nav Archit 114:221–240
4. Nethercote WCE (1981) Motions and bending moments of a warship design. Trans R Inst Nav Archit 123:352–375
5. Watanabe I, Keno M, Sawada H (1989) Effect of bow flare on shape to wave loads of a container ship. J Soc Nav Archit Jpn 166:259–266
6. O'Dea J, Powers E, Zselecsky J (1992) Experimental determination of non-linearities in vertical plane ship motions. Proceedings of the 19th Symposium on Naval Hydrodynamics, Seoul, Korea, pp 73–91
7. Smith CS (1966) Measurements of service stresses in warships. Conference on Stresses in Service, Institute of Civil Engineers, London, pp 1–18
8. Hay B, Bourne J, Eagle A, et al (1994) Characteristics of hydrodynamic loads data for a naval combatant. In: Faltinsen O (ed) Hydroelasticity in marine hydrodynamics. Balkema, Rotterdam, pp 169–188
9. Wilson R, Paterson E, Stern F (1998) Unsteady RANS CFD method for naval combatants in waves. Proceedings of the 22nd Symposium on Naval Hydrodynamics, National Academy Press, Washington, DC, pp 532–549
10. Beck RF, Cao Y, Scorpio SM, et al (1994) Non-linear ship motion computations using the desingularized method. Proceedings of the 20th Symposium on Naval Hydrodynamics, Santa Barbara, CA, pp 227–246
11. Scorpio SM, Beck RF, Korsmeyer FT (1996) Non-linear water wave computations using a multipole accelerated, desingularized method. Proceedings of the 21st Symposium on Naval Hydrodynamics, Trondheim, pp 69–74
12. Subramani A, Beck R, Scorpio S (1998) Fully nonlinear free-surface computations for arbitrary and complex hull forms. Proceedings of the 22nd Symposium on Naval Hydrodynamics, Washington, DC, pp 47–58
13. Lin WM, Zhang S, Yue D (1996) Linear and nonlinear analysis of motions and loads of a ship with forward speed in large-amplitude waves. Proceedings of the 11th International Workshop on Water Waves and Floating Bodies. Hamburg
14. Weems K, Zhang S, Lin WM, et al (1998) Structural dynamic loadings due to impact and whipping. In: Oosterveld MWC, Tan SG (eds) Practical design of ships and mobile units (PRADS'98). Elsevier, Amsterdam, pp 79–85
15. Sclavounos PD, Kring DC, Huang YF, et al (1997) A computational method as an advanced tool for design. Trans Soc Nav Archit Mar Eng 105:375–398
16. Huang Y, Sclavounos PD (1998) Nonlinear ship motions. J Ship Res 42:120–130
17. Xia J, Wang Z (1997) Time-domain hydro-elasticity theory of ships responding to waves. J Ship Res 41:286–300
18. Fonseca N, Guedes Soares C (1998a) Time-domain analysis of large-amplitude vertical motions and wave loads. J Ship Res 42:100–113
19. Fonseca N, Guedes Soares C (1998b) Nonlinear wave-induced responses of ships in irregular seas. Proceedings of the 12th International Conference on Offshore Mechanics and Arctic Engineering (OMAE'98), ASME, New York, paper 98 0446
20. Watanabe I, Guedes Soares C (1999) Comparative study on the time-domain analysis of non-linear ship motions and loads. Mar Struct 12:153–170
21. Guedes Soares C, Brown DT, Cariou A, et al (1997) Loads. In: Moan T, Berge S (eds) Proceedings of the 13th International Ship and Offshore Structures Congress (ISSC'97). Elsevier Science, London, vol 1, pp 59–122
22. Jensen JJ, Beck RF, Du S, et al (2000) Extreme hull girder loading. In: Ohtsubo H, Sumi Y (eds) Proceedings of the 14th International Ship and Offshore Structures Congress (ISSC'2000). 2–6 October. Elsevier Science, London, vol 2, pp 236–320
23. ITTC (1978) 15th ITTC Seakeeping Committee Report, Proceedings of the 15th ITTC, The Hague
24. ITTC (1981) 16th ITTC Seakeeping Committee Report, Proceedings of the 16th ITTC, Leningrad